HHS Public Access
Author manuscript
Circulation. Author manuscript; available in PMC 2021 December 08.

Published in final edited form as:
Circulation. 2020 December 08; 142(23): 2262–2275. doi:10.1161/CIRCULATIONAHA.120.047999.

Development of a Cardiac Sarcomere Functional Genomics Platform to Enable Scalable Interrogation of Human *TNNT2* Variants

Anthony M. Pettinato, B.S.[1], **Feria A. Ladha, M.S.**[1], **David J. Mellert, Ph.D.**[2], **Nicholas Legere, B.S.**[2], **Rachel Cohn, M.S.**[2], **Robert Romano, B.S.**[1], **Ketan Thakar, Ph.D.**[2], **Yu-Sheng Chen, Ph.D.**[2], **J. Travis Hinson, M.D.**[1,2,3]

[1]University of Connecticut Health Center, Farmington, CT 06030, USA

[2]The Jackson Laboratory for Genomic Medicine, Farmington, CT 06032, USA

[3]Calhoun Cardiology Center, UConn Health, Farmington, CT 06030, USA

Abstract

Background: Pathogenic *TNNT2* variants are a cause of hypertrophic (HCM) and dilated (DCM) cardiomyopathies, which promote heart failure by incompletely understood mechanisms. Additionally, the precise functional significance for 87% of *TNNT2* variants remains undetermined partially due to a lack of functional genomics studies. The knowledge of which and how *TNNT2* variants cause HCM and DCM could improve heart failure risk determination, treatment efficacy, and therapeutic discovery, as well as provide new insights into cardiomyopathy pathogenesis.

Methods: We created a toolkit of human induced pluripotent stem cell (hiPSC) models and functional assays using CRISPR/Cas9 to study *TNNT2* variant pathogenicity and pathophysiology. Using hiPSC-derived cardiomyocytes (hiPSC-CMs) in cardiac microtissue and single cell assays, we functionally interrogated 51 *TNNT2* variants, including 30 pathogenic/likely pathogenic variants and 21 variants of unknown significance (VUS). We utilized RNA-sequencing to determine the transcriptomic consequences of pathogenic *TNNT2* variants, and adapted CRISPR/Cas9 to engineer a transcriptional reporter assay to assist prediction of *TNNT2* variant pathogenicity. We also studied variant-specific pathophysiology using a thin filament-directed calcium reporter to monitor changes in myofilament calcium affinity.

Correspondence: J. Travis Hinson, MD, UConn Health and The Jackson Laboratory for Genomic Medicine, 10 Discovery Drive, Farmington, CT 06032, 860-837-2048 (t) | 860-837-2398 (f) | hinson@uchc.edu | travis.hinson@jax.org.
Author Contributions: J.T.H. and A.M.P conceived the project and designed the experiments; A.M.P. and F.A.L. performed the experiments; A.M.P., F.A.L., N.L., R.C., R.R., K.T., and Y.S.C. generated cells and/or reagents; D.J.M. developed calcium signal analysis software; A.M.P., F.A.L., and J.T.H. analyzed and interpreted the data; A.M.P. generated the figures and wrote the original draft of the manuscript; J.T.H., A.M.P., and F.A.L. revised the manuscript. All authors reviewed the manuscript prior to submission.

Disclosures
All authors declare no conflicts of interest regarding the work presented here.

Supplemental Materials
Expanded Methods
Supplemental Figures I – VII
Supplemental Excel Tables I – III
References 50–58

Results: HCM-associated *TNNT2* variants caused increased cardiac microtissue contraction, while DCM-associated variants decreased contraction. *TNNT2* variant-dependent changes in sarcomere contractile function induced graded regulation of 101 gene transcripts, including MAPK signaling targets, *HOPX*, and *NPPB*. We distinguished pathogenic *TNNT2* variants from wildtype controls using a sarcomere functional reporter engineered by inserting tdTomato into the endogenous *NPPB* locus. Based on a combination of *NPPB* reporter activity and cardiac microtissue contraction, our study provides experimental support for the reclassification of 2 pathogenic/likely pathogenic variants and 2 VUSs.

Conclusions: Our study found that HCM-associated *TNNT2* variants increased cardiac microtissue contraction, while DCM-associated variants cause decreased contraction, both of which paralleled changes in myofilament calcium affinity. Transcriptomic changes, including *NPPB* levels, directly correlated with sarcomere function and can be utilized to predict *TNNT2* variant pathogenicity.

Keywords

sarcomere; troponin T; functional genomics; cardiomyopathy; induced pluripotent stem cells; VUS; engineered heart tissues

Introduction

Genetic variant functional interpretation has lagged behind variant identification. This asymmetry has been driven by rapid improvements in the cost, scale, and accessibility of next-generation sequencing without similar breakthroughs in functional genomics. Large-scale sequencing efforts in healthy and disease human populations[1] have resulted in unintended negative consequences, including the identification of countless variants of unknown significance (VUS) for which pathogenicity cannot be precisely determined[2], and the misclassification of benign and pathogenic variants due to the lack of family-based linkage or functional assays that establish unequivocal pathogenicity[3, 4]. This incomplete genetic framework poses a significant challenge to the clinical application of genetic information and limits the value of large-scale genetic studies, unless functional genomics approaches are developed.

Heart failure (HF), a prevalent clinical syndrome with a 5-year mortality rate over 40%[5], can be caused by genetic variants in proteins comprising the cardiac sarcomere, the force producing organelle of the cardiomyocyte. Sarcomere gene variants most commonly promote HF through association with hypertrophic (HCM) and dilated cardiomyopathy (DCM), which, despite shared genetic etiology, are characterized by distinct cardiac remodeling, prognoses, and therapeutic responses[6, 7]. Because of allelic heterogeneity, sarcomere variants need to be functionally investigated in terms of not only their pathogenicity, but also whether they promote HCM, DCM, or other less common myocardial disorders[8]. A particularly challenging HF-associated sarcomere gene is cardiac troponin T (cTnT; encoded by *TNNT2*), a thin filament protein that functions in the tripartite troponin complex where calcium binds and triggers twitch force. Relative to other sarcomere genes, pathogenic *TNNT2* variants are associated with poor prognosis, as they carry increased risk of sudden cardiac death (SCD) that is disproportional to myocardial remodeling, thus confounding SCD risk prediction[9, 10]. Further complicating variant interpretations, *TNNT2* is burdened by a high proportion of VUSs (Figure 1A), as well as rare missense variants that are challenging to interpret using *in silico* methods like PolyPhen[11], especially given the lack of a complete crystal structure for the human troponin complex.

Our current knowledge regarding the functional consequences of *TNNT2* variants has focused on a small subset of *TNNT2* variants studied through *in vitro* reconstituted protein assays[12] and *in vivo* rodent models[13, 14]. These studies have implicated altered calcium sensitivity as underlying variant pathogenicity[12, 15, 16] and define a poison-peptide mechanism whereby mutant cTnT interferes with wildtype cTnT function, which can be modeled using transgenic methods. However, these approaches have been limited by model systems with non-human physiology and sarcomere protein expression[17, 18] and, most importantly, low throughput that restricts their applicability for functional interrogation of the hundreds of catalogued *TNNT2* variants.

Recently, human induced pluripotent stem cell (hiPSC) technology has enabled the generation of limitless cardiomyocytes (hiPSC-CMs) for variant modeling, which has been further enhanced by the ability to engineer isogenic models through CRISPR/Cas9 genome editing[19–21]. These technologies have been applied to analyze a sarcomere VUS in *MYL3*[22], and a more recent study combined CRISPR with dual-integrase cassette exchange to enable simultaneous generation of multiple isogenic *TNNT2* VUS models[23]. However, these approaches still remain limited by low throughput due to inefficient editing rates, long generation times, and unintended genetic and epigenetic variation, limiting applicability for functional genomics. Moreover, sarcomere functional assays to predict pathogenicity have been elusive, especially for sarcomere gene variants in which pathophysiology is less understood.

In this study, we developed a functional genomics platform (SarcTg) to study 51 *TNNT2* variants using a combination of hiPSCs, genome editing, and new functional assays. Our platform provides a carte blanche-like approach that allows for *TNNT2* variant-specific sarcomere assembly and functional interrogation, which we benchmarked against isogenic variant models. We uncovered that sarcomere contractile function exhibits graded regulation of 101 gene transcripts, including MAPK signaling targets, *HOPX*, and *NPPB*. We exploit this finding to develop a fluorescent transcriptional reporter assay to predict sarcomere functional changes induced by 51 *TNNT2* variants. Our study demonstrates that HCM and DCM-associated *TNNT2* variants result in hypercontractility and hypocontractility, respectively, in accord with an *in vivo* sarcomere tension-based model[24]. Using deviations in SarcTg platform reporter activity validated by cardiac microtissue twitch force assays, our study predicts that 6.7% of pathogenic/likely pathogenic *TNNT2* variants may be benign, while 9.5% of VUSs may be pathogenic. We also determined the pathophysiology of four well-established pathogenic *TNNT2* variants by measuring thin filament-localized calcium amplitudes. This demonstrated increased and decreased calcium affinities for HCM and DCM-associated variants, respectively, which was independent of localization to troponin C-binding sites, suggesting an allosteric-like mechanism. Our study provides a functional catalogue of *TNNT2* variants, new insights into variant pathophysiology, and a roadmap for studying other sarcomere gene variants.

Methods

No animals or human subjects were utilized in this study. Expanded Methods are provided in the Supplemental Materials. The data that support the findings of this study are available from the corresponding author upon reasonable request.

CRISPR Editing and Cardiomyocyte Differentiation

PGP1 GM23338 hiPSCs were maintained in mTeSR1 on Matrigel-coated plates and passaged with Accutase. CRISPR genome editing was performed by electroporating hiPSCs with vectors encoding Cas9, gRNA, and, where necessary, a DNA repair template, followed by clonal screening. hiPSCs were differentiated into hiPSC-CMs through modulation of Wnt/β-catenin signaling[25]. Synthetic DNA sequences are provided in Supplemental Table I.

Human Cardiac Microtissues

Cardiac microtissues were generated as previously described[19, 20]. Briefly, cantilever devices composed of polydimethylsiloxane (PDMS) were molded from SU-8 silicon masters and embedded with fluorescent microbeads for tracking. hiPSC-CMs were mixed with human cardiac fibroblasts and spun into PDMS devices containing a collagen-based ECM. Tissues were maintained in DMEM + 10% FCS. All tissue experiments included a relevant wildtype *TNNT2* control (+WT or WT/WT) to normalize for batch variation in absolute force generation. For acquisition of functional data, tissues were exposed to 1Hz pacing conditions and videos were acquired using an Andor Dragonfly equipped with a live-cell chamber and iXon EMCCD camera. Displacement of fluorescent microbeads was tracked using ImageJ.

RNA Sequencing

RNA was isolated from hiPSC-CMs using TRIzol and phenol-chloroform extraction. Sequencing libraries were prepared using the Illumina TruSeq Stranded mRNA kit and sequenced on a HiSeq 2500. Reads were aligned to the hg38 human genome using STAR, quantified with HTSeq, and analyzed using DESeq2. Gene Ontology (GO) enrichment was performed using the Broad's MSigDB. RNA-seq data is accessible through the Gene Expression Omnibus (GSE145042). Analyzed RNA-seq data is provided in Supplemental Table II.

Flow Cytometry

Flow cytometry was performed using a BD FACSymphony A5. hiPSC-CMs were stained with TO-PRO-3 and Hoechst 33342 to gate for viability and single cells, respectively, and then cell size (FSC) and tdTomato signal were determined (5,000–10,000 cells/sample). All *TNNT2* variant *NPPB*→tdTomato experiments included +WT control samples, which were used to normalize for batch variation in absolute fluorescence levels, as well as +R92Q and +R134G samples to confirm appropriate reporter response.

Calcium Transients

For calcium transients analysis, lentivirus encoding RGECO or RGECO-TnI was transduced into hiPSC-CMs of interest 2–3 days prior to analysis. For signal acquisition, cells were exposed to 1Hz pacing conditions and videos were acquired using an Andor Dragonfly. Signal time series data was generated from regions of interest in ImageJ and automated analysis was performed with a custom Python script.

Statistical Analysis

Statistical comparisons were conducted via Student's t-test or ANOVA corrected for multiple comparisons using the Holm-Sidak post-test, where indicated. Statistical significance was defined by $P \geq 0.05$ (ns), $P < 0.05$ (*), $P \leq 0.01$ (**), and $P \leq 0.001$ (***).

Results

Developing a SarcTg platform for functional interrogation of *TNNT2* variants

We set out to develop a scalable functional genomics platform to study the pathogenicity and pathophysiology of cardiac sarcomere gene variants identified in sequencing cohorts. We have previously utilized genome editing and reprogramming to generate sarcomere gene variant models in isogenic[19] and patient-specific[26] hiPSCs, respectively. Because these approaches are hindered by throughput, cost, and differentiation variability, they are limited in addressing the expanding knowledge gap regarding variant pathogenicity. Here, we focused on *TNNT2* due to the high burden of missense variants with uncertain functional significance (Figure 1A), as well as recapitulation of *in vivo* cardiomyopathy phenotypes using transgenic methods secondary to an established poison peptide mechanism[27]. We hypothesized that engineering a transgenic sarcomere platform (SarcTg) by first ablating endogenous *TNNT2* (*TNNT2*$^{-/-}$) using CRISPR/Cas9 in hiPSCs (Figure IA–C **in the** Supplement), and expressing *TNNT2* using variant-specific lentivirus (Figure 1B **and** 1C) in differentiated *TNNT2*$^{-/-}$ hiPSC-CMs could serve as a powerful tool for *TNNT2* variant functional testing. Because SarcTg hiPSC-CMs have sarcomeres composed of a single *TNNT2* variant, functional interrogation can be studied in a scalable, variant-specific manner.

We first generated *TNNT2*$^{-/-}$ hiPSC-CMs and examined cTnT (encoded by *TNNT2*) expression and sarcomere structure, which demonstrated absence of cTnT (Figure 1D) and Z-disk structures (Figure 1E), in accord with previous *TNNT2* ablation studies[27, 28]. These sarcomere knockout (SarcKO) hiPSC-CMs can then be transduced with *TNNT2*-encoding lentivirus to express transgenic cTnT (SarcTg) and induce sarcomere organization (Figure 1D **and** 1E). Next, with our ultimate goal being to study sarcomeres with variant-specific cTnT, we optimized transgenic cTnT expression by testing different lentiviral multiplicities of infection (MOI) to identify a dose that resulted in near physiological cTnT levels. Using transgenic 3xFLAG-cTnT, which integrates into the sarcomere and can be discriminated by size from endogenous cTnT in wildtype hiPSC-CMs (Figure ID–F **in the** Supplement), we found ~1/4 and ~3/4 replacement of endogenous cTnT expression when using MOIs of 1 and 5, respectively (Figure IG **in the** Supplement). Transgenic cTnT expression levels did not vary with MOI unless cells were treated with MG-132 proteasome inhibitor[29] (Figure

IH–J **in the** Supplement). Based on these results, we proceeded with MOI of 2 for all studies, as this provided physiological-like cTnT levels.

We next studied the functional consequences of restored cTnT expression by comparing SarcKO hiPSC-CMs (+empty control lentivirus) and wildtype (WT) SarcTg hiPSC-CMs (+WT *TNNT2* lentivirus). Twitch force, a direct measure of sarcomere contractile function, was studied in a 3-dimensional cardiac microtissue (CMT) assay that resembles cardiac architecture and biomechanics (Figure 1F)[19, 20, 30]. While SarcKO CMTs produced 0 μN twitch force, SarcTg produced an average of 10 μN twitch force, as quantified by cantilever displacement (Figure 1G), demonstrating assembly of functional sarcomeres. We also investigated cellular phenotypes previously associated with sarcomere functional changes, including cell size and signaling regulation[20, 24]. SarcTg hiPSC-CMs demonstrated cellular hypertrophy relative to SarcKO (Figure 1H), in association with activation of cell signaling pathways implicated in HF hypertrophy, including Akt[31] and mitogen-activated protein kinases (MAPKs) Erk[32] and p38[33] (Figure 1I **and** 1J). In summary, we have developed a method for *TNNT2* transgene-specific sarcomere assembly, which we propose to use as a platform for functional interrogation of *TNNT2* variants.

SarcTg platform recapitulates phenotypes observed in isogenic *TNNT2* variant models

Using CRISPR/Cas9, we engineered two isogenic *TNNT2* variant models to compare to corresponding SarcTg models: HCM-associated R92Q (Arginine-92 changed to Glutamine)[9] and DCM-associated R134G (Arginine-134 changed to Glycine)[34] (Figure IIA–C **in the** Supplement). Like patients harboring these variants, we studied heterozygous models and compared to isogenic controls (WT/WT) (Figure 2A). R92Q/WT CMTs demonstrated increased twitch force, while R134G/WT CMTs exhibited decreased twitch force (Figure 2B **and** 2C), in accord with single cell contraction studies of other HCM and DCM-associated *TNNT2* variants[21, 35]. For SarcTg variant models, we generated *TNNT2* lentivirus encoding R92Q (+R92Q) and R134G (+R134G) (Figure IID **in the** Supplement), which were sequence-verified (Figure III **in the** Supplement **and** Supplemental Table III) and then transduced into SarcKO hiPSC-CMs for analysis (Figure 2D). +R92Q and +R134G SarcTg variants relative to +WT exhibited similar changes in CMT twitch force compared to isogenic models (Figure 2E **and** 2F). Additionally, +R92Q and +R134G variants demonstrated altered cell size (Figure 2G) and signaling (Figure 2H **and** 2I) in correlation with CMT contractility phenotypes. As differences in sarcomere content could explain differences in CMT contraction, we also analyzed sarcomere Z-disk length, which has been shown to be proportional to sarcomere content[36]. Average Z-disk length was increased in +R92Q and decreased in +R134G hiPSC-CMs relative to +WT controls (Figure 2J **and** 2K), suggesting that *TNNT2* function correlates with sarcomere content. Taken together, these data demonstrate that the SarcTg platform can functionally distinguish pathogenic *TNNT2* variants from controls using tissue, cellular, and molecular phenotypes associated with altered *TNNT2* function.

RNA-sequencing to identify transcriptomic consequences of *TNNT2* variants

We next set out to determine how +R92Q and +R134G SarcTg models regulate the hiPSC-CM transcriptome relative to +WT, as this could uncover how changes in sarcomere function regulate gene expression, provide new insights into *TNNT2* mutation pathogenicity, and illuminate quantitative molecular markers that could assist with variant pathogenicity determination. To do this, we produced +WT, +R92Q, and +R134G SarcTg hiPSC-CMs, harvested RNA, and performed RNA-sequencing (RNA-seq) followed by computational analyses (Supplemental Table II). Principle component analysis of biological triplicates demonstrated separation of samples by *TNNT2* variant (Figure 3A). Differential gene expression analysis of hypercontractile +R92Q samples relative to +WT control identified 171 upregulated and 83 downregulated transcripts (Figure 3B), while hypocontractile +R134G samples relative to +WT control identified 83 upregulated and 287 downregulated transcripts (Figure 3C). These expression data suggest that sarcomere activation may be a general enhancer of gene transcript levels.

We next examined differentially expressed transcripts using Gene Ontology (GO) term enrichment to understand pathways regulated by HCM and DCM-associated *TNNT2* variants. Many of the highly-enriched +R92Q-upregulated and +R134G-downregulated GO terms overlapped (Figure 3B **and** 3C, denoted with *), including those with functions in muscle contraction, myofibril assembly, and extracellular matrix (ECM), while no GO terms were highly-enriched in the inverse condition. Further examination revealed that 101 transcripts were shared between the +R92Q-upregulated and +R134G-downregulated gene sets (Figure IVA **in the** Supplement), which we propose to represent a module of sarcomere function-dependent transcripts and processes (Figure IVB **and** IVC **in the** Supplement). In accord with sarcomere function-dependent phosphorylation of Erk and p38, (Figure 2I), this module contained MAPK signaling transcripts, including *RRAS*, *FGF5*, *GNG12*, *JUN*, *GADD45G*, *FLNB*, and *JUND*, as well as *HOPX*, a transcription factor implicated in hiPSC-CM maturation and hypertrophy[37]. In summary, we employed RNA-seq and uncovered 101 gene transcripts with a graded response to sarcomere function, which suggests rheostat-like regulation of gene expression by the sarcomere.

Building on this observation, we hypothesized that *TNNT2* variant pathogenicity could be assessed using a transcriptional reporter. We started by ranking the sarcomere function-dependent module of 101 gene transcripts by Log_2 fold-change relative to +WT (Figure 3D). Overall, *NPPB*, encoding the well-established heart failure biomarker B-type natriuretic peptide (BNP)[38], was the most divergent between disease-associated *TNNT2* variants and +WT controls. In addition to qPCR validation of *NPPB* expression in SarcTg models (Figure IVD **in the** Supplement), we also confirmed that two independent isogenic R92Q/WT and R134G/WT clones had divergent *NPPB* expression relative to WT/WT samples (Figure IVE **in the** Supplement). Therefore, *NPPB* transcript levels may provide a molecular readout of sarcomere function in the setting of *TNNT2* variants.

Functional classification of 51 *TNNT2* variants using the SarcTg platform

We next examined the structural localization of *TNNT2* variants to determine how localization relates to pathogenicity (Figure 4A). Pathogenic and likely pathogenic (P/LP) *TNNT2* variants are scattered across a troponin I/C-binding domain and two tropomyosin-binding domains, including a previously-reported hotspot surrounding codon 92[12]. Conversely, *TNNT2* VUSs are found across all cTnT functional domains. While no pathogenic variants have been found in the hypervariable region, the majority of *TNNT2* VUSs reside outside of this domain, necessitating methods besides localization to confidently assess VUS pathogenicity.

Using our previous observation that *NPPB* transcript levels in R92Q and R134G *TNNT2* variants deviate from WT in accord with contractility changes, we expanded the capabilities of the SarcTg platform by producing a *NPPB* reporter to functionally test a large panel of *TNNT2* variants. We utilized CRISPR/Cas9 to insert tdTomato at the transcriptional start site of one allele of *NPPB* in SarcKO hiPSCs (*NPPB*→tdTomato) to maintain *NPPB* transcriptional regulatory sequences and preserve an unedited *NPPB* allele (Figure 4B **and** Figure VA–E **in the** Supplement). We then differentiated *NPPB*→tdTomato reporter SarcKO hiPSCs to hiPSC-CMs. We observed that tdTomato fluorescent intensity in single hiPSC-CMs could be discriminated from unedited controls using flow cytometry (Figure 4C), and +R92Q and +R134G divergently altered tdTomato levels relative to +WT (Figure 4D). We also confirmed that tdTomato reporter levels were not influenced by lentiviral transduction, as empty control lentivirus did not shift reporter activity relative to non-infected hiPSC-CMs (Figure VF **in the** Supplement) and was not altered by varied MOIs (Figure VG **in the** Supplement). Additionally, generation of the *NPPB*→tdTomato reporter in a wildtype (*TNNT2*$^{+/+}$) background demonstrated deviation of variants from +WT controls, though to a lesser degree than the SarcKO (*TNNT2*$^{-/-}$) background (Figure 4E).

We also generated additional *NPPB* promoter-based reporters using both lentiviral transgenesis and CRISPR/Cas9 modification of the AAVS1 safe-harbor locus. We designed the human *NPPB* promoter sequence from open chromatin analysis using the assay for transposase-accessible chromatin with sequencing (ATAC-seq), which was performed on our control hiPSC-CMs (Figure VIA **in the** Supplement). We utilized the lentiviral (Figure VIB–E **in the** Supplement) and AAVS1 (Figure VIF–N **in the** Supplement) reporters to confirm that the *NPPB* promoter sequence alone was sufficient for *TNNT2* variant discrimination. The lentiviral reporter also supported that the SarcKO background enables better variant discrimination compared to a wildtype background and isogenic models (Figure 4E **and** Figure VID–E **in the** Supplement). Together, these results suggest that disruption of one *NPPB* allele induced by generating a *NPPB*→tdTomato at the *NPPB* locus does not diminish reporter functions, as all reporter formats distinguish variants to a similar degree. These reporter systems expand our sarcomere functional genomics toolbox and provide alternative reporter formats for the biomedical community.

Using the *NPPB*→tdTomato SarcTg platform, we then functionally interrogated 30 *TNNT2* P/LP variants listed in ClinVar. We produced lentiviruses encoding these variants (Figure III **in the** Supplement **and** Supplemental Table III) and individually transduced them into *NPPB*→tdTomato SarcKO hiPSC-CMs, followed by flow cytometry quantification of tdTomato intensity. Of 11 DCM-associated P/LP variants, all resulted in decreased *NPPB*→tdTomato intensity relative to +WT controls, while 17 out of 19 HCM-associated P/LP variants resulted in increased *NPPB*→tdTomato intensity (Figure 4F). We conclude that the SarcTg platform predicts 93.3% pathogenicity for a panel of P/LP *TNNT2* variants, as defined by significant deviation in *NPPB*→tdTomato intensity relative to WT control, with HCM and DCM-associated variants producing increased and decreased *NPPB*→tdTomato signal, respectively.

We next evaluated 21 VUSs using the *NPPB*→tdTomato SarcTg platform. Because VUSs are clinically non-actionable, classifying these variants to either benign or pathogenic would have significant clinical impact for individuals harboring these variants. Relative to +WT, 19 out of 21 VUSs (90.5%) resulted in unchanged *NPPB*→tdTomato intensity, suggesting that these variants functionally resemble wildtype *TNNT2*, while +K97N and +K258I resulted in increased *NPPB*→tdTomato, suggesting that these variants functionally resemble HCM-like *TNNT2* (Figure 4G). We then segmented all variants by ExAC[39] allele frequency to examine the relationship between population allele count and *NPPB*→tdTomato signal (Figure 4H **and** 4I). We first noted that the majority of *TNNT2* variants tested in this study were extremely rare, with 0 or 1 allele count in ExAC. Additionally, while all *TNNT2* variants that had >1 count functionally resembled wildtype *TNNT2* (=*NPPB*), so did 15.6% of 0 count variants. This suggests that allele frequency alone may only be predictive of benign classification for the minority of *TNNT2* variants that are >1 allele count in ExAC.

To validate reclassified variants, we utilized the CMT assay for SarcTg twitch force quantification. We first confirmed that four additional *TNNT2* pathogenic variants (+E160Δ[9], +I79N[35], +K210Δ[40], and +R141W[16]), which exhibited divergent *NPPB*→tdTomato expression, also resulted in divergent CMT twitch force (Figure 4J **and** 4K). Additionally, the +K97N and +K258I VUSs exhibited HCM-like twitch force while +L178F exhibited WT-like twitch force (Figure 4L **and** 4M), in accord with *NPPB*→tdTomato expression. Finally, both +I211T and +N269K, which are classified as LP in ClinVar, resulted in WT-like *NPPB*→tdTomato signal and CMT twitch force (Figure 4N **and** 4O). In summary, we identified that 6.7% of P/LP pathogenic *TNNT2* variants tested here produce wildtype-like sarcomere function; 90.5% of *TNNT2* VUSs produce wildtype-like sarcomere function, and 9.5% of *TNNT2* VUSs produce HCM-like sarcomere function.

Pathogenic *TNNT2* variants modulate thin filament Ca^{2+} affinity

To understand the pathophysiology of *TNNT2* variants, we expanded the capabilities of the SarcTg platform to include detection of Ca^{2+} transients. We first produced lentivirus encoding a recently described thin filament-directed Ca^{2+} reporter, which utilizes troponin I (TnI; encoded by *TNNI3*) fused to the RGECO fluorescent calcium sensor (RGECO-TnI)[41] (Figure 5A). Transduced RGECO-TnI in hiPSC-CMs appropriately localized to thin filament structures and fluorescence intensity cyclically-activated in a verapamil-dependent manner (Figure 5B–D). We next co-transduced *TNNT2* variants and RGECO-TnI into either *TNNT2*$^{+/+}$ or *TNNT2*$^{-/-}$ hiPSC-CMs. HCM-associated +R92Q and +E160Δ variants resulted in increased RGECO-TnI Ca^{2+} amplitudes relative to +WT, while DCM-associated +R134G and +K210Δ variants exhibited decreased amplitudes (Figure 5E–5G). Of note, while K210Δ is localized to the troponin I/C-binding domain, R134G is localized to the tropomyosin-binding domain, suggesting that RGECO-TnI Ca^{2+} amplitude changes may not relate to direct physical interaction between mutant cTnT residues and troponin C. Additionally, the HCM-like +K97N VUS also demonstrated increased RGECO-TnI Ca^{2+}

amplitudes (Figure 5H), suggesting that increased thin filament-directed Ca^{2+} amplitudes may be a common characteristic of hypercontractility-associated *TNNT2* variants.

As RGECO-TnI Ca^{2+} amplitude measurements could be confounded by differences in troponin complex assembly (Figure 2K), we also verified variant phenotypes in a wildtype (*TNNT2*$^{+/+}$) background (Figure 5F), and assessed the influence of region of interest (ROI) geometry (rectangles or lines) and size (~4–16 µm^2) on RGECO-TnI Ca^{2+} amplitudes. For both ROI geometries, the HCM-associated +R92Q *TNNT2* variant similarly increased thin filament Ca^{2+} amplitude relative to +WT (Figure VIIA **and** VIIB **in the** Supplement), and ROI size did not influence reporter signal (Figure VIIC **in the** Supplement). To assess total cellular Ca^{2+} transients to compare to RGECO-TnI results, we then transduced hiPSC-CMs with unfused RGECO, which distributes throughout the cell and cyclically-activates in a verapamil-dependent manner (Figure VIID–G **in the** Supplement), though cellular Ca^{2+} amplitudes were unchanged between *TNNT2* variants and +WT controls (Figure VIIH–J **in the** Supplement). In summary, these results suggest that pathogenic *TNNT2* variants result in altered thin filament-localized Ca^{2+} amplitudes that correlate with contractility changes, but are independent of mutation structural localization and overall cellular Ca^{2+} amplitudes.

Discussion

Pathogenic *TNNT2* variants are an inheritable risk factor for heart failure, yet we have an incomplete understanding of the pathogenicity and pathophysiology of the majority of variants. Secondary to low population allele counts, absence of linkage studies, and high frequency of missense variants that are challenging to assess by *in silico* methods, only 13% of *TNNT2* variants in ClinVar are currently denoted with high-confidence ACMG classifications[42] of benign or pathogenic (Figure 1A). Even likely pathogenic variants, which may impact clinical decision making for individuals harboring these variants, could have unacceptably-high 10% false positive rates[3]. The development of an accurate genetic framework for *TNNT2* variants has also been hindered by allelic heterogeneity. In *TNNT2*, which is illustrative of many sarcomere genes, different variants may result in heart failure through HCM, DCM, or other myocardial disorders—each with different treatment responses and prognoses. Because of an incomplete understanding of how specific *TNNT2* variants result in HCM or DCM, functional assay development has also been challenging.

In this study, we utilized genome-engineered hiPSC-CMs, transcriptomics, and multi-scale functional assays to understand the pathogenicity and pathophysiology of 51 *TNNT2* variants. We focused on *TNNT2*, in part, because it is amenable to transgenic variant modeling through a poison-peptide mechanism[16, 27] that enables high-efficiency variant delivery into hiPSC-CMs using lentivirus. We optimized this transgenic approach, which we call SarcTg, to provide physiologic-like cTnT expression levels, and also benchmarked SarcTg variants against isogenic models of established HCM and DCM-associated *TNNT2* variants. Like R92Q transgenic mice[14] and our isogenic models, we observed that HCM-associated R92Q SarcTg hiPSC-CMs exhibit hypercontractility that was similarly observed with two additional HCM mutations, E160Δ and I79N. In contrast, we observed hypocontractility in DCM-associated R134G, K210Δ, and R141W. These contractility phenotypes are reminiscent of previous studies of other sarcomere mutations in cardiac microtissues from our group[19, 20] and the work of others in mice[16, 24]. This dichotomy in sarcomere function was also reflected in hypertrophic signaling responses and transcriptomic changes, as we uncovered 101 transcripts that exhibited a graded response to *TNNT2*-dependent sarcomere function, including MAPK signaling targets and the transcription factor *HOPX*.

Among differential transcripts, *NPPB* levels were most predictive of *TNNT2* variant pathogenicity irrespective of modeling approach (transgenic or isogenic) or genetic background (with or without wildtype cTnT). *NPPB* encodes for the secreted peptide hormone BNP, which is a well-established biomarker for heart failure prognosis and treatment responses[43]. We found *NPPB* levels correlated with "inside-out" mechanical inputs derived from *TNNT2*-dependent sarcomere functional changes. *In vivo*, BNP levels are concordantly elevated in heart failure due to HCM or DCM, which can likely be explained by a combination of intrinsic and extrinsic inputs on BNP, such as neurohormonal signaling[44] and increased "outside-in" mechanical inputs from wall stress due to elevated cardiac filling pressures[45] that are excluded from our *in vitro* assays.

To screen 51 *TNNT2* variants, we engineered SarcTg *NPPB*→tdTomato reporter hiPSC-CMs and quantified reporter activity by flow cytometry. We determined that 28 out of 30 pathogenic/likely-pathogenic *TNNT2* variants could be discriminated from wildtype *TNNT2*, as HCM-associated variants enhanced reporter levels while DCM-associated variants diminished it. Only I211T and N269K were indistinguishable from wildtype *TNNT2*, and these variants have only been reported in small studies from non-European ancestry[46]. Based on this experimental evidence, we estimate that up to 6.7% of pathogenic/likely-pathogenic *TNNT2* variants may be benign. We also tested 21 VUSs, with two resulting in an HCM-like increase in reporter signal and 19 producing wildtype-like signal. We also observed that all *TNNT2* variants with >1 ExAC allele count produced benign-like reporter signal. While lower ExAC allele frequency correlated with pathogenicity, most variants were identified with ≤1 count, and we observed several wildtype-like *TNNT2* variants with allele counts of 0. This demonstrates that allele frequency alone is insufficient for high-confidence *TNNT2* variant classification. Finally, to assess *TNNT2* variant-specific pathophysiology, we tested myofilament-directed calcium transients for R92Q, E160Δ, R134G, and K210Δ. Concordant with cardiac microtissue force changes, R92Q and E160Δ increased, while R134G and K210Δ decreased myofilament-directed calcium transients. Taken together, we propose that the molecular basis for these pathogenic *TNNT2* variants may be alterations in thin filament-directed calcium affinity, which results in corresponding changes in thin filament activation and force production. Finally, we developed new tools for sharing with the biomedical community including both a *NPPB*→tdTomato lentiviral reporter and AAVS1 safe-harbor reporter.

Our study has important limitations, including the utilization of hiPSC-CMs, which resemble neonatal human cardiomyocytes in gene expression and function. For example, hiPSC-CMs express skeletal troponin I (*TNNI1*), while adult human cardiomyocytes express cardiac troponin I (*TNNI3*)[47]. *TNNI1* relative to *TNNI3* has been shown to exhibit differences in myofilament calcium sensitivity and adrenergic responsiveness that could impact functional studies[48]. Additionally, while we benchmarked SarcTg models against isogenic models of well-established mutations in a heterozygous background, it is possible that functional interpretation of some variants could also be affected by co-expression with wildtype cTnT and from transgenic issues such as changes in expression levels. The SarcTg platform also does not have the capacity to detect aberrant RNA splicing phenotypes secondary to *TNNT2* missense variants. Unlike in *LMNA*[49], *TNNT2* missense mutations have not been shown to affect RNA splicing to the best of our knowledge. In addition, we recognize that variant pathogenicity cannot be confidently classified based on a single experimental study. Our study utilized the *NPPB* reporter and cardiac microtissue functional assays, but some pathogenic *TNNT2* variants may alter other cTnT functions not assayed here, thus additional experimental and clinical studies will need to be performed prior to definitive *TNNT2* variant reclassification.

Future directions of this study will be directed at functional interrogation of the entire catalogue of 384 *TNNT2* variants listed in ClinVar. It will also be critically important to study sex-dependence and ethnicity-dependence of *TNNT2* variant phenotypes, such as by developing the SarcTg platform in a female or non-European ancestry line. Finally, with the capacity to generate patient-specific *TNNT2* variant models, we can begin to assess variant-specific treatment responses and pathophysiology.

In summary, we demonstrate a functional catalogue of 51 *TNNT2* variants studied in hiPSC-CMs and cardiac microtissues. HCM-associated mutations cause hypercontractility while DCM-associated mutations cause hypocontractility. Our study provides experimental evidence based on *NPPB* reporter and cardiac microtissue functional assays that two pathogenic/likely-pathogenic *TNNT2* variants resemble wildtype cTnT and two *TNNT2* VUSs resemble HCM-associated *TNNT2* variants. We observe that the underlying pathophysiology of several pathogenic *TNNT2* variants is altered myofilament calcium affinity. Finally, our study provides a roadmap and new tools for future sarcomere functional genomics studies.

Supplementary Material

Refer to Web version on PubMed Central for supplementary material.

Acknowledgements

We thank Anthony Carcio and Tiffany Prosio (The Jackson Laboratory for Genomic Medicine) for expertise in flow cytometry, Bo Reese (UConn Center for Genome Innovation) for expertise in RNA sequencing, and James Grady (UConn Health Biostatistics Core) for consultation regarding statistical analyses. Artwork in Figure 1 was created, in part, with images from BioRender.

Sources of Funding

This work was supported, in part, by the National Institutes of Health (HL125807, HL142787, and EB028898 to J.T.H.), American Heart Association (PRE34381021 to A.M.P. and PRE35110005 to F.A.L.), and institutional support from the University of Connecticut and Jackson Laboratory for Genomic Medicine.

Non-standard Abbreviations and Acronyms:

CRISPR	clustered regularly interspaced short palindromic repeats

cTnT	cardiac troponin T protein
DCM	dilated cardiomyopathy
HCM	hypertrophic cardiomyopathy
hiPSC	human induced pluripotent stem cell
hiPSC-CM	hiPSC-derived cardiomyocyte
NPPB	gene encoding brain natriuretic peptide
RGECO	red genetically encoded calcium indicator
REGCO-TnI	RGECO fused to cardiac troponin I
SarcKO	*TNNT2* knockout hiPSC-CMs
SarcTg	SarcKO hiPSC-CMs transduced with *TNNT2* lentivirus
TNNT2	gene encoding cardiac troponin T
VUS	variants of unknown significance

References

1. Lek M, Karczewski KJ, Minikel EV, Samocha KE, Banks E, Fennell T, O'Donnell-Luria AH, Ware JS, Hill AJ, Cummings BB, et al. Analysis of protein-coding genetic variation in 60,706 humans. Nature. 2016;536:285–91. doi: 10.1038/nature19057. [PubMed: 27535533]
2. Morales A and Hershberger RE. Variants of Uncertain Significance: Should We Revisit How They Are Evaluated and Disclosed? Circ Genom Precis Med. 2018;11:e002169. doi: 10.1161/CIRCGEN.118.002169. [PubMed: 29848615]
3. Harrison SM and Rehm HL. Is 'likely pathogenic' really 90% likely? Reclassification data in ClinVar. Genome Med. 2019;11:72. doi: 10.1186/s13073-019-0688-9. [PubMed: 31752965]
4. Hoffman-Andrews L The known unknown: the challenges of genetic variants of uncertain significance in clinical practice. J Law Biosci. 2017;4:648–657. doi: 10.1093/jlb/lsx038. [PubMed: 29868193]
5. Virani SS, Alonso A, Benjamin EJ, Bittencourt MS, Callaway CW, Carson AP, Chamberlain AM, Chang AR, Cheng S, Delling FN, et al. Heart Disease and Stroke Statistics-2020 Update: A Report From the American Heart Association. Circulation. 2020;141:e139–e596. doi: 10.1161/CIR.0000000000000757. [PubMed: 31992061]
6. Marian AJ and Braunwald E. Hypertrophic Cardiomyopathy: Genetics, Pathogenesis, Clinical Manifestations, Diagnosis, and Therapy. Circ Res. 2017;121:749–770. doi: 10.1161/CIRCRESAHA.117.311059. [PubMed: 28912181]
7. McNally EM and Mestroni L. Dilated Cardiomyopathy: Genetic Determinants and Mechanisms. Circ Res. 2017;121:731–748. doi: 10.1161/CIRCRESAHA.116.309396. [PubMed: 28912180]
8. Klaassen S, Probst S, Oechslin E, Gerull B, Krings G, Schuler P, Greutmann M, Hurlimann D, Yegitbasi M, Pons L, et al. Mutations in sarcomere protein genes in left ventricular noncompaction. Circulation. 2008;117:2893–901. doi: 10.1161/CIRCULATIONAHA.107.746164. [PubMed: 18506004]
9. Watkins H, McKenna WJ, Thierfelder L, Suk HJ, Anan R, O'Donoghue A, Spirito P, Matsumori A, Moravec CS, Seidman JG, et al. Mutations in the genes for cardiac troponin T and alpha-tropomyosin in hypertrophic cardiomyopathy. N Engl J Med. 1995;332:1058–64. doi: 10.1056/NEJM199504203321603. [PubMed: 7898523]

10. O'Mahony C, Elliott P and McKenna W. Sudden cardiac death in hypertrophic cardiomyopathy. Circ Arrhythm Electrophysiol. 2013;6:443–51. doi: 10.1161/CIRCEP.111.962043. [PubMed: 23022709]
11. Adzhubei IA, Schmidt S, Peshkin L, Ramensky VE, Gerasimova A, Bork P, Kondrashov AS and Sunyaev SR. A method and server for predicting damaging missense mutations. Nat Methods. 2010;7:248–9. doi: 10.1038/nmeth0410-248. [PubMed: 20354512]
12. Gangadharan B, Sunitha MS, Mukherjee S, Chowdhury RR, Haque F, Sekar N, Sowdhamini R, Spudich JA and Mercer JA. Molecular mechanisms and structural features of cardiomyopathy-causing troponin T mutants in the tropomyosin overlap region. Proc Natl Acad Sci U S A. 2017;114:11115–11120. doi: 10.1073/pnas.1710354114. [PubMed: 28973951]
13. Du CK, Morimoto S, Nishii K, Minakami R, Ohta M, Tadano N, Lu QW, Wang YY, Zhan DY, Mochizuki M, et al. Knock-in mouse model of dilated cardiomyopathy caused by troponin mutation. Circ Res. 2007;101:185–94. doi: 10.1161/CIRCRESAHA.106.146670. [PubMed: 17556660]
14. Tardiff JC, Hewett TE, Palmer BM, Olsson C, Factor SM, Moore RL, Robbins J and Leinwand LA. Cardiac troponin T mutations result in allele-specific phenotypes in a mouse model for hypertrophic cardiomyopathy. J Clin Invest. 1999;104:469–81. doi: 10.1172/JCI6067. [PubMed: 10449439]
15. Morimoto S, Lu QW, Harada K, Takahashi-Yanaga F, Minakami R, Ohta M, Sasaguri T and Ohtsuki I. Ca(2+)-desensitizing effect of a deletion mutation Delta K210 in cardiac troponin T that causes familial dilated cardiomyopathy. Proc Natl Acad Sci U S A. 2002;99:913–8. doi: 10.1073/pnas.022628899. [PubMed: 11773635]
16. Ramratnam M, Salama G, Sharma RK, Wang DW, Smith SH, Banerjee SK, Huang XN, Gifford LM, Pruce ML, Gabris BE, et al. Gene-Targeted Mice with the Human Troponin T R141W Mutation Develop Dilated Cardiomyopathy with Calcium Desensitization. PLoS One. 2016;11:e0167681. doi: 10.1371/journal.pone.0167681. [PubMed: 27936050]
17. Robinson P, Griffiths PJ, Watkins H and Redwood CS. Dilated and hypertrophic cardiomyopathy mutations in troponin and alpha-tropomyosin have opposing effects on the calcium affinity of cardiac thin filaments. Circ Res. 2007;101:1266–73. doi: 10.1161/CIRCRESAHA.107.156380. [PubMed: 17932326]
18. Ford SJ, Mamidi R, Jimenez J, Tardiff JC and Chandra M. Effects of R92 mutations in mouse cardiac troponin T are influenced by changes in myosin heavy chain isoform. J Mol Cell Cardiol. 2012;53:542–51. doi: 10.1016/j.yjmcc.2012.07.018. [PubMed: 22884844]
19. Cohn R, Thakar K, Lowe A, Ladha FA, Pettinato AM, Romano R, Meredith E, Chen YS, Atamanuk K, Huey BD, et al. A Contraction Stress Model of Hypertrophic Cardiomyopathy due to Sarcomere Mutations. Stem Cell Reports. 2019;12:71–83. doi: 10.1016/j.stemcr.2018.11.015. [PubMed: 30554920]
20. Hinson JT, Chopra A, Nafissi N, Polacheck WJ, Benson CC, Swist S, Gorham J, Yang L, Schafer S, Sheng CC, et al. HEART DISEASE. Titin mutations in iPS cells define sarcomere insufficiency as a cause of dilated cardiomyopathy. Science. 2015;349:982–6. doi: 10.1126/science.aaa5458. [PubMed: 26315439]
21. Sun N, Yazawa M, Liu J, Han L, Sanchez-Freire V, Abilez OJ, Navarrete EG, Hu S, Wang L, Lee A, et al. Patient-specific induced pluripotent stem cells as a model for familial dilated cardiomyopathy. Sci Transl Med. 2012;4:130ra47. doi: 10.1126/scitranslmed.3003552.
22. Ma N, Zhang JZ, Itzhaki I, Zhang SL, Chen H, Haddad F, Kitani T, Wilson KD, Tian L, Shrestha R, et al. Determining the Pathogenicity of a Genomic Variant of Uncertain Significance Using CRISPR/Cas9 and Human-Induced Pluripotent Stem Cells. Circulation. 2018;138:2666–2681. doi: 10.1161/CIRCULATIONAHA.117.032273. [PubMed: 29914921]
23. Lv W, Qiao L, Petrenko N, Li W, Owens AT, McDermott-Roe C and Musunuru K. Functional Annotation of TNNT2 Variants of Uncertain Significance With Genome-Edited Cardiomyocytes. Circulation. 2018;138:2852–2854. doi: 10.1161/CIRCULATIONAHA.118.035028. [PubMed: 30565988]
24. Davis J, Davis LC, Correll RN, Makarewich CA, Schwanekamp JA, Moussavi-Harami F, Wang D, York AJ, Wu H, Houser SR, et al. A Tension-Based Model Distinguishes Hypertrophic versus

Dilated Cardiomyopathy. Cell. 2016;165:1147–1159. doi: 10.1016/j.cell.2016.04.002. [PubMed: 27114035]

25. Lian X, Zhang J, Azarin SM, Zhu K, Hazeltine LB, Bao X, Hsiao C, Kamp TJ and Palecek SP. Directed cardiomyocyte differentiation from human pluripotent stem cells by modulating Wnt/beta-catenin signaling under fully defined conditions. Nat Protoc. 2013;8:162–75. doi: 10.1038/nprot.2012.150. [PubMed: 23257984]
26. Hinson JT, Chopra A, Lowe A, Sheng CC, Gupta RM, Kuppusamy R, O'Sullivan J, Rowe G, Wakimoto H, Gorham J, et al. Integrative Analysis of PRKAG2 Cardiomyopathy iPS and Microtissue Models Identifies AMPK as a Regulator of Metabolism, Survival, and Fibrosis. Cell Rep. 2016;17:3292–3304. doi: 10.1016/j.celrep.2016.11.066. [PubMed: 28009297]
27. Ahmad F, Banerjee SK, Lage ML, Huang XN, Smith SH, Saba S, Rager J, Conner DA, Janczewski AM, Tobita K, et al. The role of cardiac troponin T quantity and function in cardiac development and dilated cardiomyopathy. PLoS One. 2008;3:e2642. doi: 10.1371/journal.pone.0002642. [PubMed: 18612386]
28. Karakikes I, Termglinchan V, Cepeda DA, Lee J, Diecke S, Hendel A, Itzhaki I, Ameen M, Shrestha R, Wu H, et al. A Comprehensive TALEN-Based Knockout Library for Generating Human-Induced Pluripotent Stem Cell-Based Models for Cardiovascular Diseases. Circ Res. 2017;120:1561–1571. doi: 10.1161/CIRCRESAHA.116.309948. [PubMed: 28246128]
29. Solomon V and Goldberg AL. Importance of the ATP-ubiquitin-proteasome pathway in the degradation of soluble and myofibrillar proteins in rabbit muscle extracts. J Biol Chem. 1996;271:26690–7. doi: 10.1074/jbc.271.43.26690. [PubMed: 8900146]
30. Hinson JT, Chopra A, Lowe A, Sheng CC, Gupta RM, Kuppusamy R, O'Sullivan J, Rowe G, Wakimoto H, Gorham J, et al. Integrative Analysis of PRKAG2 Cardiomyopathy iPS and Microtissue Models Identifies AMPK as a Regulator of Metabolism, Survival, and Fibrosis. Cell Rep. 2016;17:3292–3304. doi: 10.1016/j.celrep.2016.11.066. [PubMed: 28009297]
31. Matsui T, Nagoshi T and Rosenzweig A. Akt and PI 3-kinase signaling in cardiomyocyte hypertrophy and survival. Cell Cycle. 2003;2:220–3. doi: [PubMed: 12734428]
32. Bueno OF and Molkentin JD. Involvement of extracellular signal-regulated kinases 1/2 in cardiac hypertrophy and cell death. Circ Res. 2002;91:776–81. doi: 10.1161/01.res.0000038488.38975.1a. [PubMed: 12411391]
33. Wang Y, Huang S, Sah VP, Ross J Jr., Brown JH, Han J and Chien KR. Cardiac muscle cell hypertrophy and apoptosis induced by distinct members of the p38 mitogen-activated protein kinase family. J Biol Chem. 1998;273:2161–8. doi: 10.1074/jbc.273.4.2161. [PubMed: 9442057]
34. Hershberger RE, Pinto JR, Parks SB, Kushner JD, Li D, Ludwigsen S, Cowan J, Morales A, Parvatiyar MS and Potter JD. Clinical and functional characterization of TNNT2 mutations identified in patients with dilated cardiomyopathy. Circ Cardiovasc Genet. 2009;2:306–13. doi: 10.1161/CIRCGENETICS.108.846733. [PubMed: 20031601]
35. Wang L, Kim K, Parikh S, Cadar AG, Bersell KR, He H, Pinto JR, Kryshtal DO and Knollmann BC. Hypertrophic cardiomyopathy-linked mutation in troponin T causes myofibrillar disarray and pro-arrhythmic action potential changes in human iPSC cardiomyocytes. J Mol Cell Cardiol. 2018;114:320–327. doi: 10.1016/j.yjmcc.2017.12.002. [PubMed: 29217433]
36. Dabiri GA, Turnacioglu KK, Sanger JM and Sanger JW. Myofibrillogenesis visualized in living embryonic cardiomyocytes. Proc Natl Acad Sci U S A. 1997;94:9493–8. doi: 10.1073/pnas.94.17.9493. [PubMed: 9256510]
37. Friedman CE, Nguyen Q, Lukowski SW, Helfer A, Chiu HS, Miklas J, Levy S, Suo S, Han JJ, Osteil P, et al. Single-Cell Transcriptomic Analysis of Cardiac Differentiation from Human PSCs Reveals HOPX-Dependent Cardiomyocyte Maturation. Cell Stem Cell. 2018;23:586–598 e8. doi: 10.1016/j.stem.2018.09.009. [PubMed: 30290179]
38. Logeart D, Thabut G, Jourdain P, Chavelas C, Beyne P, Beauvais F, Bouvier E and Solal AC. Predischarge B-type natriuretic peptide assay for identifying patients at high risk of re-admission after decompensated heart failure. J Am Coll Cardiol. 2004;43:635–41. doi: 10.1016/j.jacc.2003.09.044. [PubMed: 14975475]
39. Karczewski KJ, Weisburd B, Thomas B, Solomonson M, Ruderfer DM, Kavanagh D, Hamamsy T, Lek M, Samocha KE, Cummings BB, et al. The ExAC browser: displaying reference data

information from over 60 000 exomes. Nucleic Acids Res. 2017;45:D840–D845. doi: 10.1093/nar/gkw971. [PubMed: 27899611]

40. Kamisago M, Sharma SD, DePalma SR, Solomon S, Sharma P, McDonough B, Smoot L, Mullen MP, Woolf PK, Wigle ED, et al. Mutations in sarcomere protein genes as a cause of dilated cardiomyopathy. N Engl J Med. 2000;343:1688–96. doi: 10.1056/NEJM200012073432304. [PubMed: 11106718]
41. Sparrow AJ, Sievert K, Patel S, Chang YF, Broyles CN, Brook FA, Watkins H, Geeves MA, Redwood CS, Robinson P, et al. Measurement of Myofilament-Localized Calcium Dynamics in Adult Cardiomyocytes and the Effect of Hypertrophic Cardiomyopathy Mutations. Circ Res. 2019;124:1228–1239. doi: 10.1161/CIRCRESAHA.118.314600. [PubMed: 30732532]
42. Richards S, Aziz N, Bale S, Bick D, Das S, Gastier-Foster J, Grody WW, Hegde M, Lyon E, Spector E, et al. Standards and guidelines for the interpretation of sequence variants: a joint consensus recommendation of the American College of Medical Genetics and Genomics and the Association for Molecular Pathology. Genet Med. 2015;17:405–24. doi: 10.1038/gim.2015.30. [PubMed: 25741868]
43. Tsutamoto T, Wada A, Maeda K, Hisanaga T, Maeda Y, Fukai D, Ohnishi M, Sugimoto Y and Kinoshita M. Attenuation of compensation of endogenous cardiac natriuretic peptide system in chronic heart failure: prognostic role of plasma brain natriuretic peptide concentration in patients with chronic symptomatic left ventricular dysfunction. Circulation. 1997;96:509–16. doi: 10.1161/01.cir.96.2.509. [PubMed: 9244219]
44. Majalahti T, Suo-Palosaari M, Sarman B, Hautala N, Pikkarainen S, Tokola H, Vuolteenaho O, Wang J, Paradis P, Nemer M, et al. Cardiac BNP gene activation by angiotensin II in vivo. Mol Cell Endocrinol. 2007;273:59–67. doi: 10.1016/j.mce.2007.05.003. [PubMed: 17587490]
45. de Bold AJ, Bruneau BG and Kuroski de Bold ML. Mechanical and neuroendocrine regulation of the endocrine heart. Cardiovasc Res. 1996;31:7–18. doi: [PubMed: 8849584]
46. Kassem H, Azer RS, Saber-Ayad M, Moharem-Elgamal S, Magdy G, Elguindy A, Cecchi F, Olivotto I and Yacoub MH. Early results of sarcomeric gene screening from the Egyptian National BA-HCM Program. J Cardiovasc Transl Res. 2013;6:65–80. doi: 10.1007/s12265-012-9425-0. [PubMed: 23233322]
47. Bedada FB, Chan SS, Metzger SK, Zhang L, Zhang J, Garry DJ, Kamp TJ, Kyba M and Metzger JM. Acquisition of a quantitative, stoichiometrically conserved ratiometric marker of maturation status in stem cell-derived cardiac myocytes. Stem Cell Reports. 2014;3:594–605. doi: 10.1016/j.stemcr.2014.07.012. [PubMed: 25358788]
48. Fentzke RC, Buck SH, Patel JR, Lin H, Wolska BM, Stojanovic MO, Martin AF, Solaro RJ, Moss RL and Leiden JM. Impaired cardiomyocyte relaxation and diastolic function in transgenic mice expressing slow skeletal troponin I in the heart. J Physiol. 1999;517 (Pt 1):143–57. doi: 10.1111/j.1469-7793.1999.0143z.x. [PubMed: 10226156]
49. Ito K, Patel PN, Gorham JM, McDonough B, DePalma SR, Adler EE, Lam L, MacRae CA, Mohiuddin SM, Fatkin D, et al. Identification of pathogenic gene mutations in LMNA and MYBPC3 that alter RNA splicing. Proc Natl Acad Sci U S A. 2017;114:7689–7694. doi: 10.1073/pnas.1707741114. [PubMed: 28679633]
50. Tohyama S, Hattori F, Sano M, Hishiki T, Nagahata Y, Matsuura T, Hashimoto H, Suzuki T, Yamashita H, Satoh Y, et al. Distinct metabolic flow enables large-scale purification of mouse and human pluripotent stem cell-derived cardiomyocytes. Cell Stem Cell. 2013;12:127–37. doi: 10.1016/j.stem.2012.09.013. [PubMed: 23168164]
51. Kutner RH, Zhang XY and Reiser J. Production, concentration and titration of pseudotyped HIV-1-based lentiviral vectors. Nat Protoc. 2009;4:495–505. doi: 10.1038/nprot.2009.22. [PubMed: 19300443]
52. Chenouard N, Smal I, de Chaumont F, Maska M, Sbalzarini IF, Gong Y, Cardinale J, Carthel C, Coraluppi S, Winter M, et al. Objective comparison of particle tracking methods. Nat Methods. 2014;11:281–9. doi: 10.1038/nmeth.2808. [PubMed: 24441936]
53. Steger C An unbiased detector of curvilinear structures. IEEE Transactions on Pattern Analysis and Machine Intelligence. 1998;20:113–125. doi: 10.1109/34.659930.

54. Liberzon A, Subramanian A, Pinchback R, Thorvaldsdottir H, Tamayo P and Mesirov JP. Molecular signatures database (MSigDB) 3.0. Bioinformatics. 2011;27:1739–40. doi: 10.1093/bioinformatics/btr260. [PubMed: 21546393]
55. Subramanian A, Tamayo P, Mootha VK, Mukherjee S, Ebert BL, Gillette MA, Paulovich A, Pomeroy SL, Golub TR, Lander ES, et al. Gene set enrichment analysis: a knowledge-based approach for interpreting genome-wide expression profiles. Proc Natl Acad Sci U S A. 2005;102:15545–50. doi: 10.1073/pnas.0506580102. [PubMed: 16199517]
56. Ashburner M, Ball CA, Blake JA, Botstein D, Butler H, Cherry JM, Davis AP, Dolinski K, Dwight SS, Eppig JT, et al. Gene ontology: tool for the unification of biology. The Gene Ontology Consortium. Nat Genet. 2000;25:25–9. doi: 10.1038/75556. [PubMed: 10802651]
57. The Gene Ontology C The Gene Ontology Resource: 20 years and still GOing strong. Nucleic Acids Res. 2019;47:D330–D338. doi: 10.1093/nar/gky1055. [PubMed: 30395331]
58. Benjamini Y, Krieger AM and Yekutieli D. Adaptive linear step-up procedures that control the false discovery rate. Biometrika. 2006;93:491–507. doi: 10.1093/biomet/93.3.491.

Clinical Perspective

What is new?

- We developed a scalable human cardiomyocyte platform to functionally interrogate *TNNT2* variants previously identified in the human population.
- Transcriptome analysis of pathogenic HCM-associated and DCM-associated *TNNT2* variants revealed molecular signatures of cardiomyopathy pathogenicity.
- Through engineering a human cardiomyocyte *NPPB* reporter assay, we functionally interrogated 30 HCM- and DCM-associated *TNNT2* variants, as well as 21 variants of uncertain significance (VUS), which provided experimental evidence to support the reclassification of some *TNNT2* pathogenic variants and VUSs that were additionally validated in cardiac microtissue functional assays.

What are the clinical implications?

- Inheritance of pathogenic *TNNT2* variants is a leading cause of cardiomyopathy.
- The majority of *TNNT2* variants identified in the human population are classified as VUSs, which limits the clinical utility of genetic testing.
- Reclassification of *TNNT2* variants would improve cardiomyopathy risk determination and treatment responses for individuals harboring these variants.

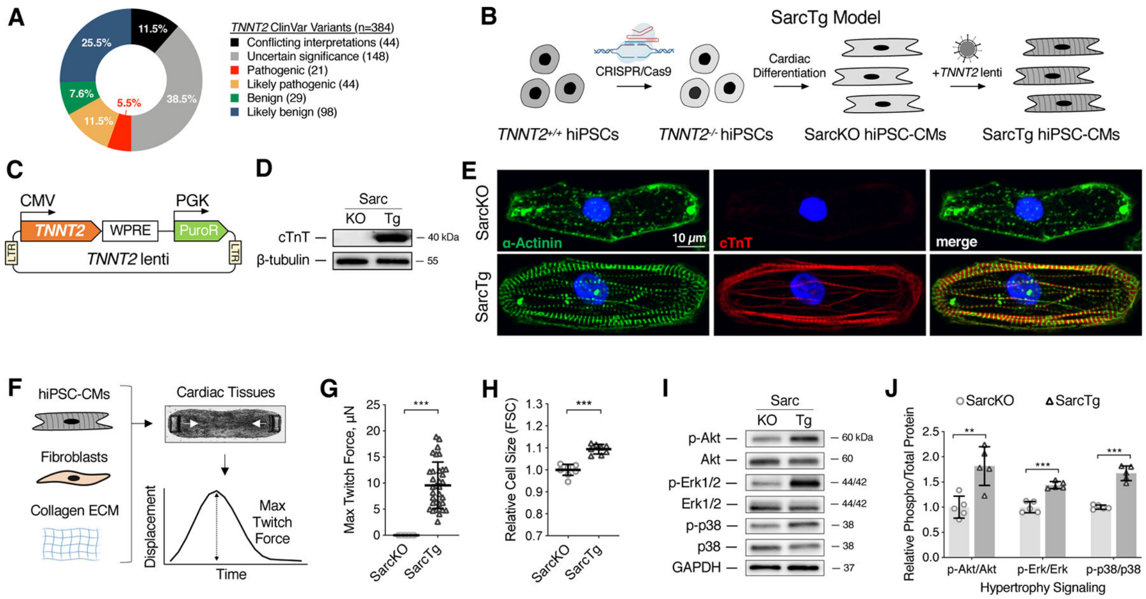

Figure 1. Developing a SarcTg platform for functional interrogation of *TNNT2* variants.
(A) Classification of the 384 *TNNT2* variants catalogued in NIH ClinVar (Dec. 2019).
(B) Overview of strategy for production of SarcTg hiPSC-CMs from CRISPR-engineered *TNNT2*$^{-/-}$ hiPSC-CMs (SarcKO) utilizing lentiviral *TNNT2* to generate transgene-specific sarcomeres (SarcTg).
(C) Schematic of lentiviral vector used for delivery of *TNNT2* for SarcTg studies.
(D) Representative protein immunoblot of cardiac troponin T (cTnT) expression in SarcTg and SarcKO hiPSC-CMs.
(E) Representative confocal micrograph of hiPSC-CMs immunostained for cardiac α-actinin (green), cTnT (red), and DAPI (blue) to visualize sarcomere structure in SarcTg and SarcKO hiPSC-CMs.
(F) General overview of cardiac microtissue (CMT) assay.
(G) Max twitch force generated by CMTs assembled from SarcKO (+empty lentivirus) versus SarcTg (+WT *TNNT2* lentivirus) hiPSC-CMs (n=24–34 individual tissues generated across 5 independently transduced hiPSC-CM differentiation batches).
(H) Quantification of SarcTg hiPSC-CM cell size relative to SarcKO using forward scatter (FSC) from flow cytometry (n=8–9 independent transductions).
(I) Representative protein immunoblots and (J) quantification of phosphorylated and total Akt, Erk1/2, and p38 to assess cardiac hypertrophy signaling (n=5 independent transductions).
Data are mean ± SD; significance assessed by Student's t-test and defined by $P \leq 0.01$ (**) and $P \leq 0.001$ (***).

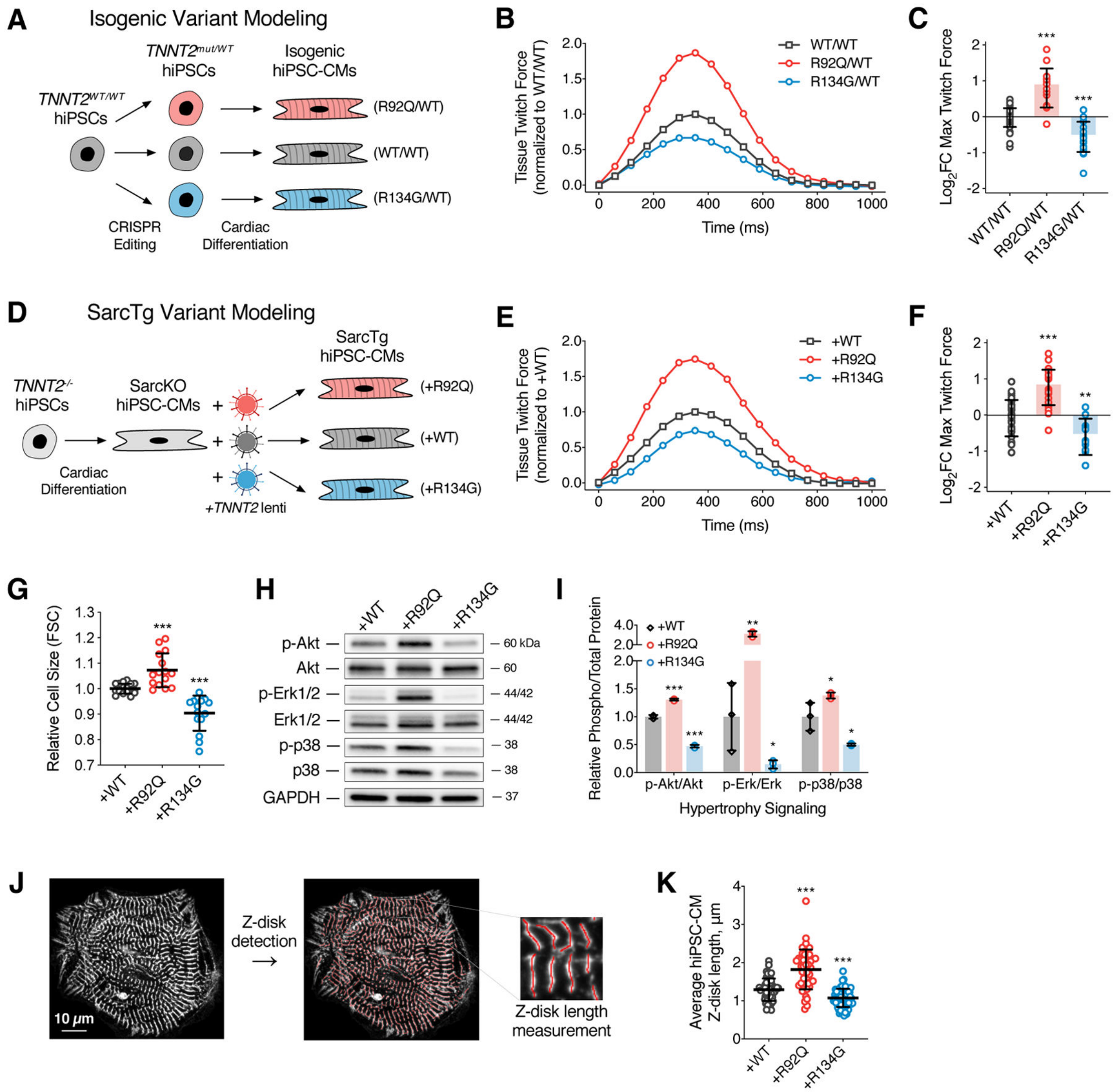

Figure 2. SarcTg platform recapitulates phenotypes observed in isogenic *TNNT2* variant models

(A) Overview of isogenic *TNNT2* variant modeling strategy, which utilizes CRISPR/Cas9 to independently knock-in pathogenic variants into wildtype control hiPSCs, followed by independent differentiation into hiPSC-CMs for analysis.

(B) Representative tracings and **(C)** quantification of the Log_2 fold-change (Log_2FC) in twitch force produced by CMTs assembled from isogenic R92Q/WT and R134G/WT hiPSC-CMs relative to WT/WT control (n=18–40 individual tissues generated across 5 hiPSC-CM differentiation batches; one isogenic clone was used for each variant).

(D) Overview of SarcTg variant modeling, which involves lentiviral delivery of *TNNT2* variants into SarcKO hiPSC-CMs.

(E) Representative tracings and **(F)** quantification of the Log_2FC in twitch force produced by CMTs assembled from +R92Q and +R134G SarcTg hiPSC-CMs relative to +WT control (n=11–34 individual tissues generated across 5 independently transduced hiPSC-CM differentiation batches).

(G) Quantification of +R92Q and +R134G cell size relative to +WT control SarcTg hiPSC-CMs using forward scatter (FSC) from flow cytometry (n=15–18 independent transductions).

(H) Representative protein immunoblots and (I) quantification of phosphorylated and total Akt, Erk1/2, and p38 in SarcTg variant hiPSC-CMs (n=3 independent transductions).

(J) Representative confocal micrograph of hiPSC-CMs immunostained for cardiac α-actinin and **(K)** subjected to ridge detection to quantify Z-disk length of +WT, +R92Q, and +R134G SarcTg hiPSC-CMs (n=48–71 cells per variant).

Data are mean ± SD; significance assessed by ANOVA using Holm-Sidak correction for multiple comparisons to control (+WT or WT/WT) and defined by $P < 0.05$ (*), $P \leq 0.01$ (**), and $P \leq 0.001$ (***).

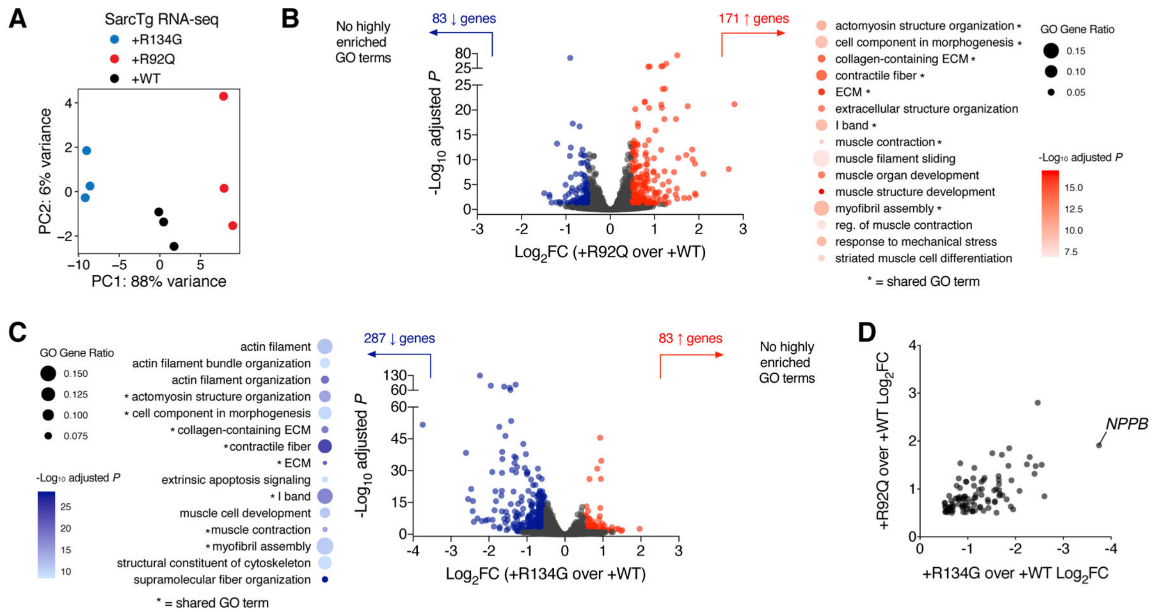

Figure 3. RNA-sequencing to identify transcriptomic consequences of *TNNT2* variants.

(A) Principle component analysis plot of RNA sequencing performed on +WT, +R92Q, and +R134G SarcTg hiPSC-CMs (n=3 independent transductions). The percent variance explained by PC1 (88%) and PC2 (6%) are each listed on the respective axes.

(B) Volcano plot and Gene Ontology (GO) term enrichment analysis of the significantly downregulated (blue; $Log_2FC \le -0.5$, FDR-adjusted $P < 0.05$) and upregulated (red; $Log_2FC \ge 0.5$, FDR-adjusted $P < 0.05$) genes in +R92Q SarcTg hiPSC-CMs relative to +WT, as well as **(C)** +R134G SarcTg hiPSC-CMs relative to +WT. Enriched GO terms denoted with * are shared between those upregulated in +R92Q and downregulated in +R134G.

(D) Log_2FC ranked expression of the 101 sarcomere function-dependent transcripts (see Supplemental Figure IV) that are upregulated in +R92Q (y-axis) and downregulated in +R134G (x-axis) relative to +WT control.

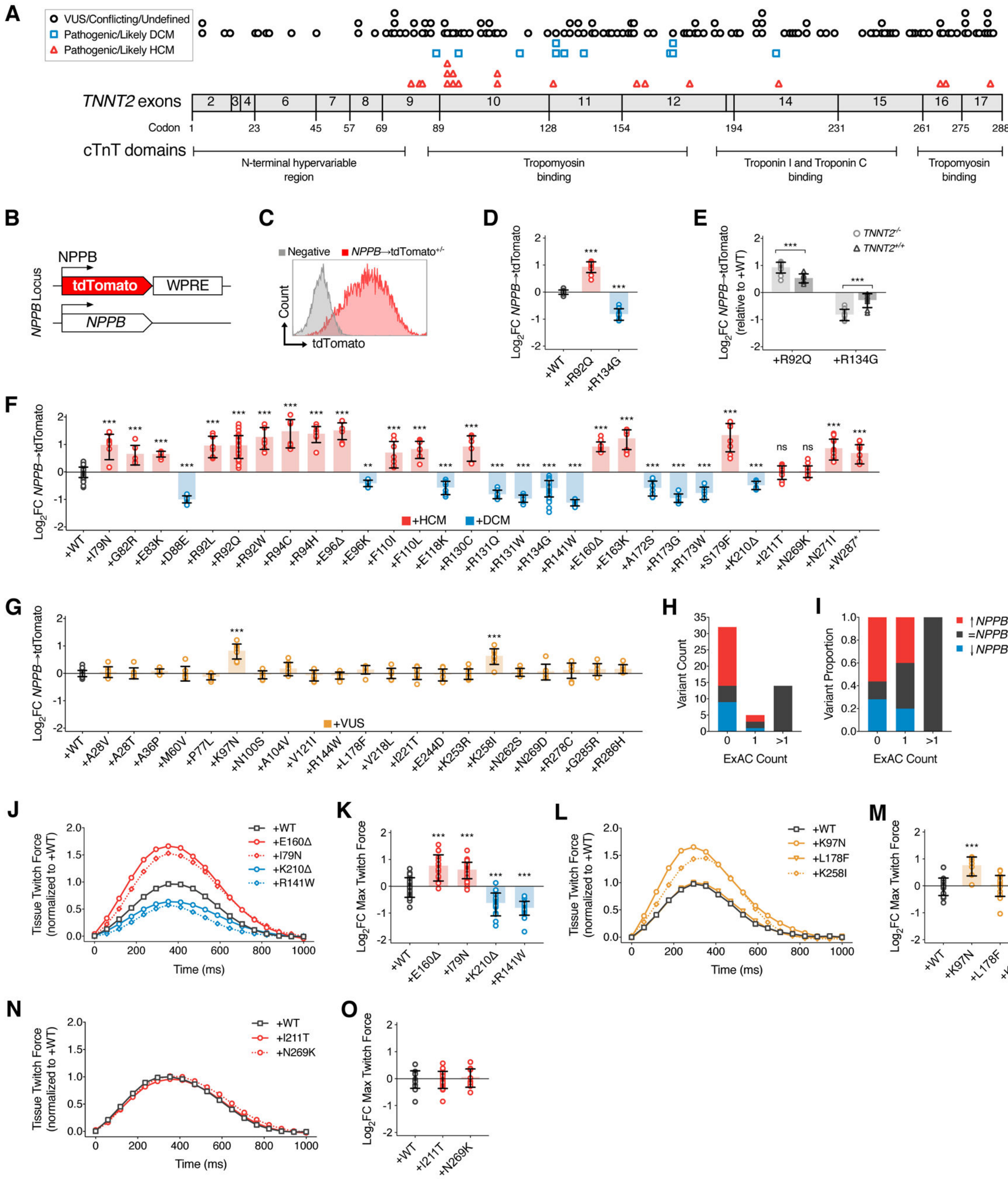

Figure 4. Functional classification of 51 *TNNT2* variants using the SarcTg platform

(A) Localization of *TNNT2* missense variants from NIH ClinVar, which are aligned along a schematic map of the canonical adult human *TNNT2* mRNA transcript (Ensembl ENST00000509001) annotated with spliced exons, codon positions, and cTnT functional domains.

(B) Simplified schematic of *NPPB*→tdTomato reporter in hiPSC-CMs.

(C) Representative histograms of tdTomato expression from flow cytometry analysis of negative control hiPSC-CMs versus *NPPB*→tdTomato hiPSC-CMs.

(D) Flow cytometry analysis of +WT, +R92Q, and +R134G SarcTg *NPPB*→tdTomato hiPSC-CMs (n=11 independent transductions).

(E) Comparison of *NPPB*→tdTomato intensity (relative to respective +WT controls) between *TNNT2* lentiviral variants transduced into SarcKO (*TNNT2*$^{-/-}$) *NPPB*→tdTomato (light grey) versus *TNNT2*$^{+/+}$ *NPPB*→tdTomato (dark grey) hiPSC-CMs (n=8–11 independent transductions).

(F) *NPPB*→tdTomato intensity (relative to +WT control) from a panel of 30 pathogenic/likely pathogenic HCM (red) and DCM (blue) *TNNT2* variants (n≥8 independent transductions per variant).

(G) *NPPB*→tdTomato intensity (relative to +WT control) from a panel of 21 *TNNT2* VUSs (yellow) (n≥8 independent transductions per variant).

(H) Counts and **(I)** proportion of *TNNT2* variants categorized by ExAC allele count and alterations in *NPPB*→tdTomato expression.

(J) Representative tracings and **(K)** quantification of twitch force produced by CMTs assembled from +E160Δ (HCM; ↑*NPPB*), +I79N (HCM; ↑*NPPB*), +K210Δ (DCM; ↓*NPPB*), and +R141W (DCM; ↓*NPPB*) SarcTg hiPSC-CMs relative to +WT (n=17–41 individual tissues generated across 5 independently transduced hiPSC-CM differentiation batches).

(L) Representative tracings and **(M)** quantification of twitch force produced by CMTs assembled from +K97N (VUS; ↑*NPPB*), +L178F (VUS; =*NPPB*), and +K258I (VUS; ↑*NPPB*) SarcTg hiPSC-CMs relative to +WT (n=7–16 individual tissues generated across 2 independently transduced hiPSC-CM differentiation batches).

(N) Representative tracings and **(O)** quantification of twitch force produced by CMTs assembled from +I211T (HCM; =*NPPB*) and +N269K (HCM; =*NPPB*) SarcTg hiPSC-CMs relative to +WT (n=14–21 individual tissues generated across 2 independently transduced hiPSC-CM differentiation batches).

Data are mean ± SD; significance assessed by Student's t-test (E) or ANOVA using Holm-Sidak correction for multiple comparisons to +WT control (D, F-O) and defined by $P < 0.05$ (*), $P \leq 0.01$ (**), and $P \leq 0.001$ (***).

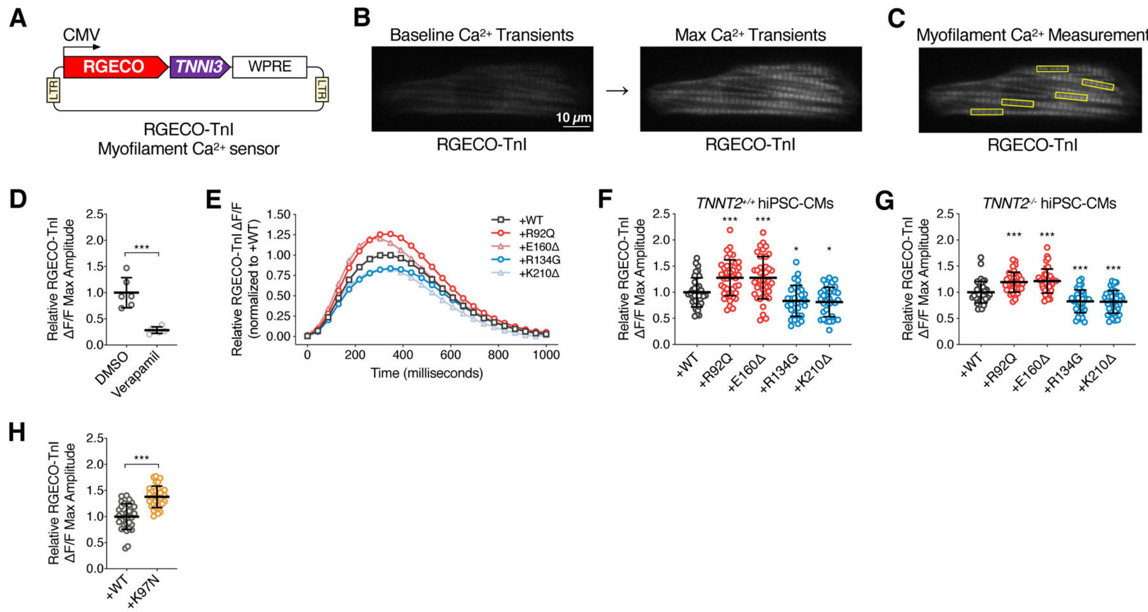

Figure 5. Pathogenic *TNNT2* variants modulate thin filament Ca^{2+} affinity.

(A) Schematic of lentiviral vector used for expression of a RGECO-TnI myofilament Ca^{2+} sensor.

(B) Example live-cell imaging frames of an hiPSC-CM transduced with RGECO-TnI lentivirus representing baseline and peak fluorescence produced by Ca^{2+} locally bound to RGECO-TnI at the sarcomere.

(C) Strategy for quantifying myofilament Ca^{2+} transients from an hiPSC-CM video, which involves measuring and averaging the signal from five independent myofibril segments per cell.

(D) Quantification of max RGECO-TnI ΔF/F amplitude produced by WT hiPSC-CMs treated with verapamil relative to DMSO vehicle (n=6 cells per condition).

(E) Representative tracings of the ΔF/F-transformed RGECO-TnI signal (relative to +WT control) produced by hiPSC-CMs transduced with HCM (+R92Q and +E160Δ) and DCM (+R134G and +K210Δ) *TNNT2* variants, and **(F)** quantification of max RGECO-TnI ΔF/F amplitude produced by pathogenic *TNNT2* variants relative to +WT control using wildtype ($TNNT2^{+/+}$) and **(G)** SarcKO ($TNNT2^{-/-}$) hiPSC-CM backgrounds (n=32–41 cells per variant).

(H) Quantification of max RGECO-TnI ΔF/F amplitude produced by the +K97N variant relative to +WT control using the SarcKO hiPSC-CM background (n=32 cells per variant). Data are mean ± SD; significance assessed by Student's t-test (D, H) or ANOVA using Holm-Sidak correction for multiple comparisons to +WT control (F, G) and defined by $P \leq 0.01$ (**) and $P \leq 0.001$ (***).